Supporting Information for:

Role of nanoscale hydroxyapatite in disease suppression of *Fusarium*-infected tomato

Chuanxin Ma[1, 2], Qingqing Li[3], Weili Jia[4], Heping Shang[3], Jian Zhao[5], Yi Hao[1], Chunyang Li[3], Mason Tomko[3], Nubia Zuverza-Mena[2], Wade, Elmer[6], Jason C. White[2, *], Baoshan Xing[3]

[1]Key Laboratory for City Cluster Environmental Safety and Green Development of the Ministry of Education, Institute of Environmental and Ecological Engineering, Guangdong University of Technology, Guangzhou 510006, China

[2]The Connecticut Agricultural Experiment Station, New Haven, CT 06504, USA; Jason.White@ct.gov

[3]Stockbridge School of Agriculture, University of Massachusetts Amherst, Amherst, MA 01003, USA

[4]SCNU Environmental Research Institute, Guangdong Provincial Key Laboratory of Chemical Pollution and Environmental Safety & MOE Key Laboratory of Theoretical Chemistry of Environment, South China Normal University, Guangzhou 510006, China

[5]Institute of Coastal Environmental Pollution Control, Key Laboratory of Marine Environment and Ecology, Ministry of Education, and Frontiers Science Center for Deep Ocean Multispheres and Earth System, Ocean University of China, Qingdao 266100, China

[6]Department of Plant Pathology and Ecology, The Connecticut Agricultural Experiment Station, New Haven, Connecticut 06504, United States

Number of Pages: **20**

Number of Figures: **13**

Number of Tables: **0**

Section S1. SEM observation

Leaf tissues after foliar exposure to nHA suspensions were freeze-dried in a lyophilizer. Particle distribution on tomato leaf surfaces across all seven treatments, including control, 0.3 mM nHA-L, 1.5 mM nHA-L, 0.3 mM nHA-S, 1.5 mM nHA-S, 1.5 mM $CaHPO_4$ and 1.5 mM nHA-C, was examined by scanning electron microscopy (SEM, S-4800, Hitachi, Japan). The element distribution of P and Ca was further confirmed by energy dispersive X-ray spectroscopy (EDS, INCA 100, Oxfordshire, U.K.).[1,2]

Section S2. Antioxidant enzymatic activity[3,4]

Peroxidase (POD) was extracted in 50 mM phosphate (pH 7.0) containing 1% (w/v) polyvinylpyrrolidone. Briefly, 50 μL of enzyme extract was mixed with reaction buffer containing 1.75 mL of 50 mM sodium phosphate buffer (pH 7.0) and 0.1 mL of 4% guaiacol in a cuvette. One hundred microliters of 1% (v/v) H_2O_2 was used to initiate the reaction. Increased absorbance was recorded at 470 nm for 2 min.

Polyphenol oxidase (PPO) was extracted in the same buffer as for POD extraction. The reaction mixture consisted of 200 μL of enzyme extract and 2.8 mL of 10 mM catechol. PPO activity was recorded by measuring its ability to oxidize catechol at 410 nm.

Phenylalanin ammonialyase (PAL) was extracted in 0.1 M sodium borate buffer (pH 8.8). One hundred μL of enzyme extract was used to react with 2.9 mL of reaction buffer containing 100 mM sodium borate buffer (pH 8.8) and 50 mM 1-phenylalanine at 37 °C for 1 hr. The change in absorbance at 298 nm was monitored.

Section S3. Phenolic content

Fresh tissues of shoots and roots across all treatments were ground into fine powder in liquid nitrogen and weighed into a conical tube containing 80% methanol (*v/v*). The mixture was shaken at room temperature for 12 h and then centrifuged at 2000 *g* for 10 min. Fifty μL of supernatant

as mixed with 450 μL of deionized water and 250 μL of 2 M Folin-Ciocalteu reagent. The mixture was then incubated in 1.25 mL of 20 g/L Na_2CO_3 solution at 25 °C for 20 min. The absorbance of the mixture was measured at 735 nm using a UV-Vis spectrometer.[5]

Section S4. Phytohormone measurement

The procedures for phytohormone extraction and detection were that of Shang et al. (2020) with minor modification. Briefly, tomato tissues were ground in liquid nitrogen and weighed into a 15 mL centrifuge tube containing 4 mL mixed solvent of 2-propanol/H_2O/concentrated HCl (2:1:0.002, *v/v/v*). All samples were shaken in an ice bath at 120 rpm for 30 min. Then, 4 mL dichloromethane were added and the samples were then shaken in an ice bath for another 30 min. After centrifugation at 5000 rpm at 4 °C for 10 min, the organic layer was collected and concentrated under nitrogen flow. The concentrated samples were re-dissolved in 1.5 mL of CH_3OH/H_2O (8:2, *v/v*) for phytohormone and phytoalexin measurement using high performance liquid chromatography equipped with UV-Vis detector (HPLC; UV-Vis detector model: SPD-M20A; SHIMADZU, Kyoto, Japan). The column (C6-Phenyl 110A) temperature was set at 25 °C. The detection wavelength was 190 nm. For mobile phase, solvent A was H_2O with 0.1% HCOOH and solvent B was CH_3CN. The elution program was 20% solvent B for 15 min, followed by a linear gradient from 20% to 100% B in 20 min, and finally holding at 100% B for 5 min.[6]

Section S5. Fatty acid measurement

Approximately 0.2-0.3 g of fresh root or shoot tissue was weighed into 15 mL conical tubes containing 2.5 mL of methanol acidified by H_2SO_4 (2.5%, *v/v*). All samples were derivatized at 80 °C for 1 h and were then cooled down to ambient temperature. Two mL of deionized water and 3 mL of hexane were added, followed by vigorous shaking for 30 min to extract fatty acid methyl esters (FAMEs). The extract was separated from the water phase by centrifugation at 3000 rpm for 5 min.[7] The extraction step was repeated once to ensure an adequate recovery. The

collected extract was concentrated under N_2 and was then re-suspended in 2 mL (root) or 5 mL (shoot) of dichloromethane (CH_2Cl_2). FAMEs analysis was done by gas chromatography–mass spectrometry (GC-MS; GCMS-QP2010 Ultra, Shimadzu, Kyoto, Japan) using an integrated guard column (Rtx-5MS, 30 m in length, 0.25 mm in diameter, 0.25 μm in thickness, Shimadzu, Kyoto, Japan). The sample injection volume was 1 μL under splitless mode with helium carrier gas. The injection, ion-source, and interface temperature were 250, 200, and 300 °C, respectively. The thermal program was as follows: the column oven temperature was at 80 °C and increased at 3 °C/min to 290 °C. spectra were recorded within a m/z range from 40 to 450.[8] FAMEs standard compounds were purchased from AccuStandard, Inc. (New Haven, CT).

Section S6 Gene expression analysis

FOL infected shoot and root fresh tissues of randomly selected three biological replicates in each nHA treatment were ground into fine powder in liquid nitrogen. The total RNA in shoots and roots was isolated by using a Sigma-Aldrich Spectrum Plant Total RNA kit and its concentration and quality were measured by a Thermo Scientific Nanodrop Lite Spectrophotometer. A Verso cDNA synthesis kit was used to synthesis complementary DNA (cDNA) by using one microgram of the extracted RNA as template. The synthesized cDNA was diluted to 50 ng/μL, which was used as the template for the following qPCR analysis. Primers of three genes important to plant defense; polyphenol oxidase (PPO), PTI5 (a transcriptional regulator for multiple defense genes) and PR1A1 (plant resistance protein) were designed and synthesized using qPCR primer design tool in Integrated DNA Technologies. Bio-Rad SsoAdvanced Universal SYBR Green Supermix was used to run the qPCR and the working concentration of each primer was 10 μM. The thermal program for qPCR amplification was: 95 °C for 30 s; 95 °C for 15 s, 63 °C for 30 s, repeating 40 cycles; melting curve from 65 to 95 °C. The total volume of each reaction was 20 μL and was used as a housekeeping gene for normalization. Relative expression of each gene was calculated through $2^{-\Delta\Delta Ct}$ method.[9]

Section S7. Particle distribution on leaf surfaces

After foliar exposure to different-sized nHA, SEM images were used to visualize particle distribution on leaf surfaces (**Figure S3-S5**). No particles were evident in the control samples, although some particles were randomly distributed on the surfaces in both the ionic control and commercial nHA treatments (**Figure S3**). In the large nHA treatment, some nHA aggregates were clearly evident upon exposure to both amendment concentrations; similar but smaller aggregates were observed in the small nHA treatments at both concentrations (**Figure S3**). In the large-sized high dose nHA treatment, the large particle aggregates near the trichrome were further analyzed by EDS and the results confirm P and Ca (red circle) presence, indicating the presence of nHA; similarly, commercial nHA was found near the trichomes and also confirmed by EDS (**Figure S4**). No nHA was found in or near the stomata (**Figure S5**). Overall, the current results suggest that different-sized nHA were clearly evident on the leaf surfaces but there appeared to be no specific association with any particular structure or surface feature. Similarly, Ma et al. (2019) also reported that Cu-based nanomaterials, including $Cu_3(PO_4)_2 \bullet 3H_2O$ nanosheets and CuO nanoparticles, were randomly distributed on the leaf surfaces of tomato after a dip application.[9]

Section S8. Micronutrient content

Micronutrients play important roles in the defense systems of plants.[10] In general, *FOL* infection alone tended to increase the contents of micronutrients in shoots and roots in comparison with the healthy control; foliar exposure of different sizes of nHA either had no impact on or reduced the micronutrient content of shoots and roots in both healthy and diseased groups (**Figure S7**). For example, approximately 20-30% decreases in the Cu content were evident in *FOL* infected shoots and roots upon exposure to different sizes of nHA (**Figure S7A-B**). No difference in the Fe, Zn and Mn content was noted in *FOL* infected shoots across all treatments (**Figure S7C, E and G**); however, in the diseased group, the addition of large and small nHA decreased the root Fe and Zn by approximately 40 and 30%, respectively, relative to the control (**Figure S7D and F**).

The Mn content in *FOL*-infected roots in the high dose of small nHA treatment was nearly 50% higher as compared to the diseased control (**Figure S7H**). Thus, similar to the macronutrient content, *FOL* seems to be the more significant variable than nHA when evaluating changes in micronutrient content.

Section S9. The ratio of UFA/SFA and C18:3/(C18:2+C18:0)

The ratio of unsaturated fatty acids (UFA) to saturated fatty acids (SFA) was calculated as a function of disease and nHA. UFA tends to be converted to SFA in plants under stress conditions.[11] In the shoots, the ratio of UFA/SFA was lower in the diseased group than that in the healthy group within the same nHA treatments (**Figure S12A**). It is worth noting that the lower magnitude of reduction in the UFA/SFA ratio in diseased shoots upon exposure to different-sized nHA signifies a partial alleviation of *FOL*-induced stress in tomato with the amendment (**Figure S12A**). Conversely, in the roots, slight increases in the diseased group within different-sized nHA were evident as compared to the *FOL* control (**Figure S12B**). The ratio of C18:3/(C18:2+C18:0) is another index that can be used to evaluate stress response in infected tomato upon exposure to different-sized nHA.[12] In the diseased group, exposure to both-sized nHA increased the ratio by 4-16% in shoots as compared to the *FOL* control (**Figure 12C**), indicating that the presence of nHA could induce membrane fluidity remodeling by stimulating the C18:3 level. No difference in the ratio of C18:3/(C18:2+C18:0) in the roots was evident across all the treatments regardless of the *FOL* infection (**Figure S12D**).

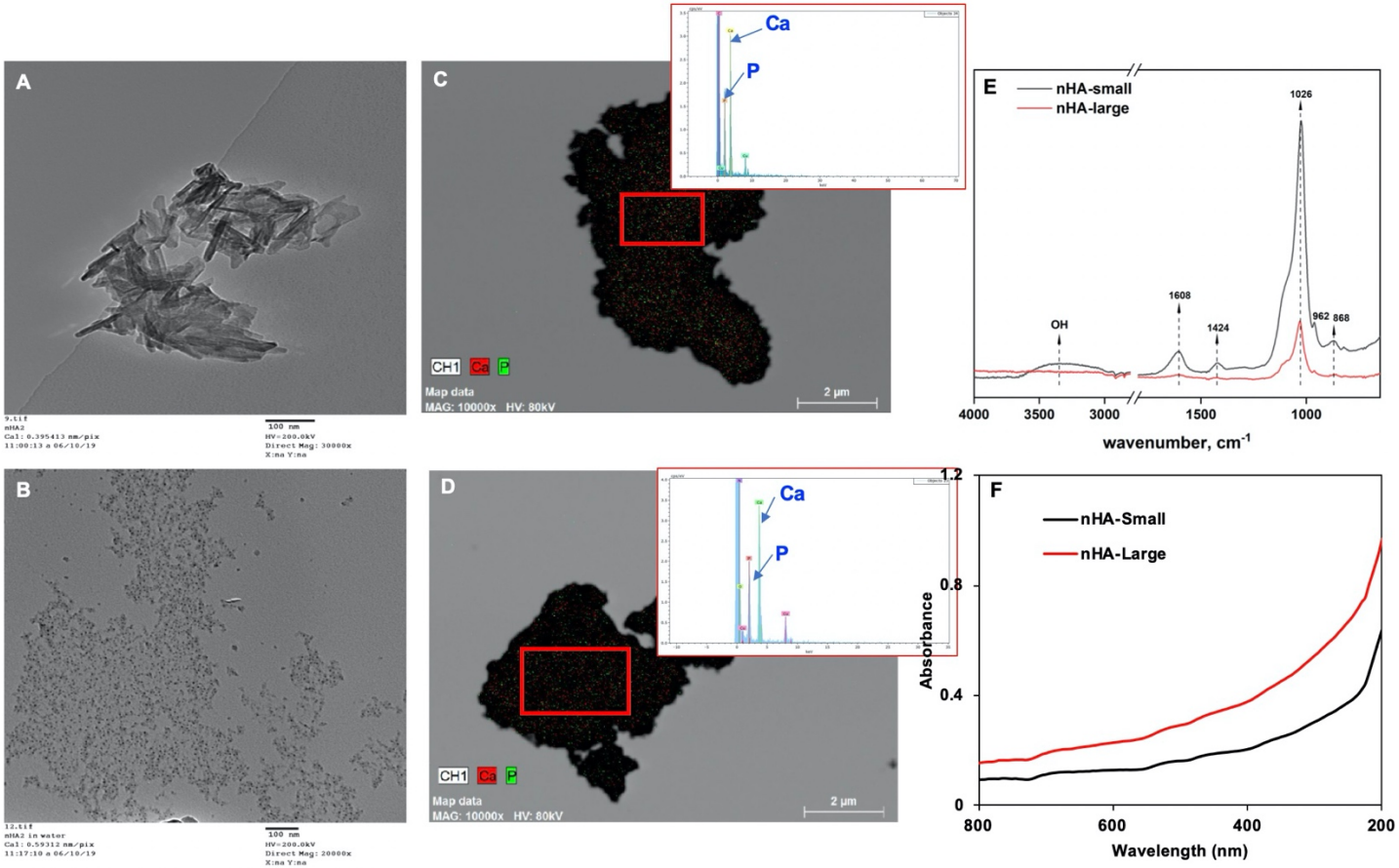

Figure S1. nHA-L and nHA-S characterization. TEM images of nHA-L (**A**) and nHA-S (**B**); Ca and P mapping and EDS of nHA-L (**C**) and nHA-S (**D**); FTIR spectra of nHA-L and nHA-S (**E**); UV-Vis spectra of nHA-L and nHA-S (**F**). Note: the insert in panel **C** and **D** represents the respective EDS spectrum of the synthesized nHA.

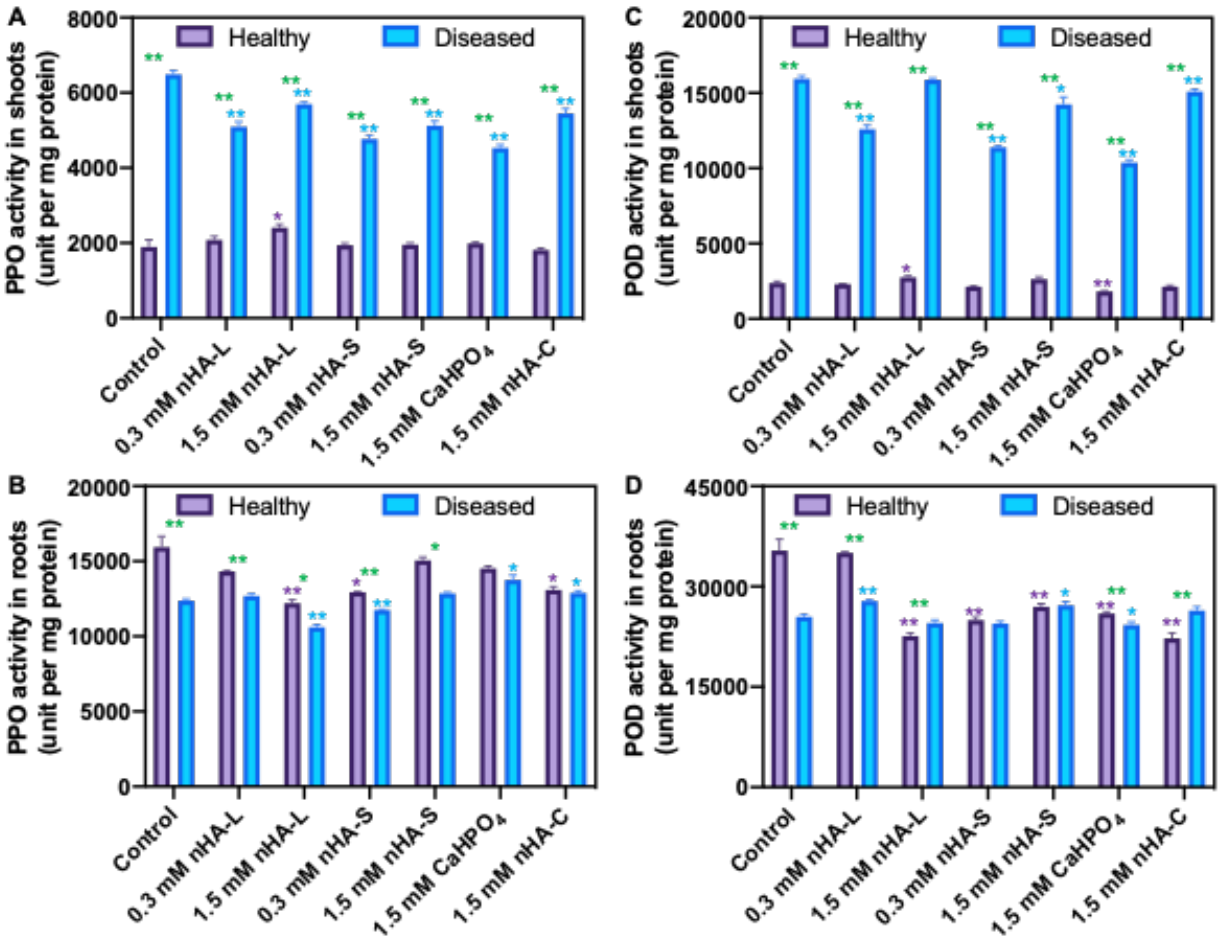

Figure S2. PPO (**A and B**) and POD (**C and D**) activity in tomato shoots and roots in healthy and diseased groups upon exposure to different sizes of nHA. In each panel, single asterisk "*" and double asterisks "**" represent significant difference at $p < 0.05$ and $p < 0.01$, respectively; in addition, asterisk in purple "*" indicates the significant difference between control and each nHA treatment within healthy group; asterisk in blue "*" indicates the significant difference between control and each nHA treatment within diseased group; asterisk in green "*" indicates the significant difference between healthy and diseased group within the same nHA treatment.

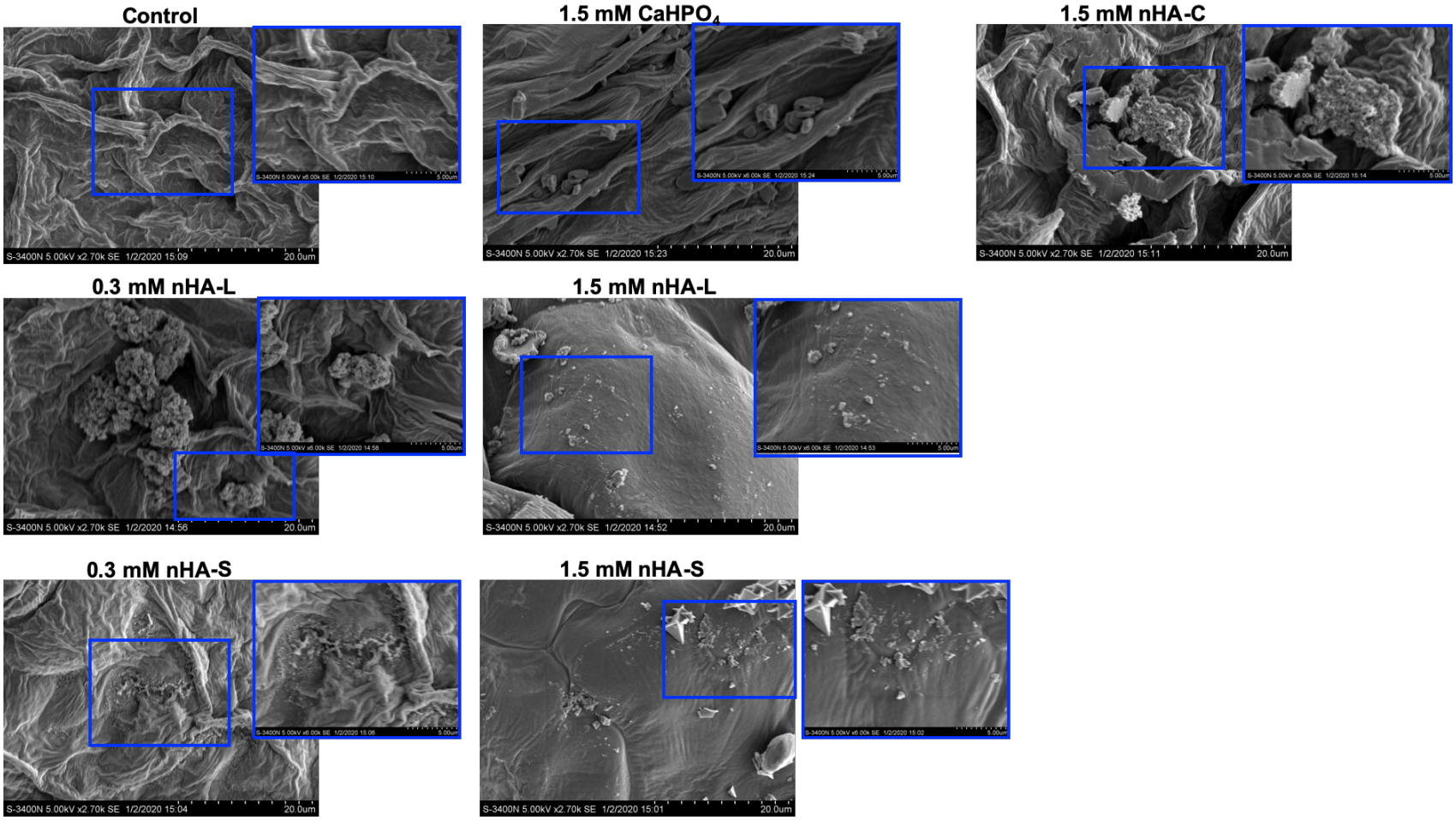

Figure S3. Particle distribution on tomato leaf surfaces after foliar application of different sizes of nHA.

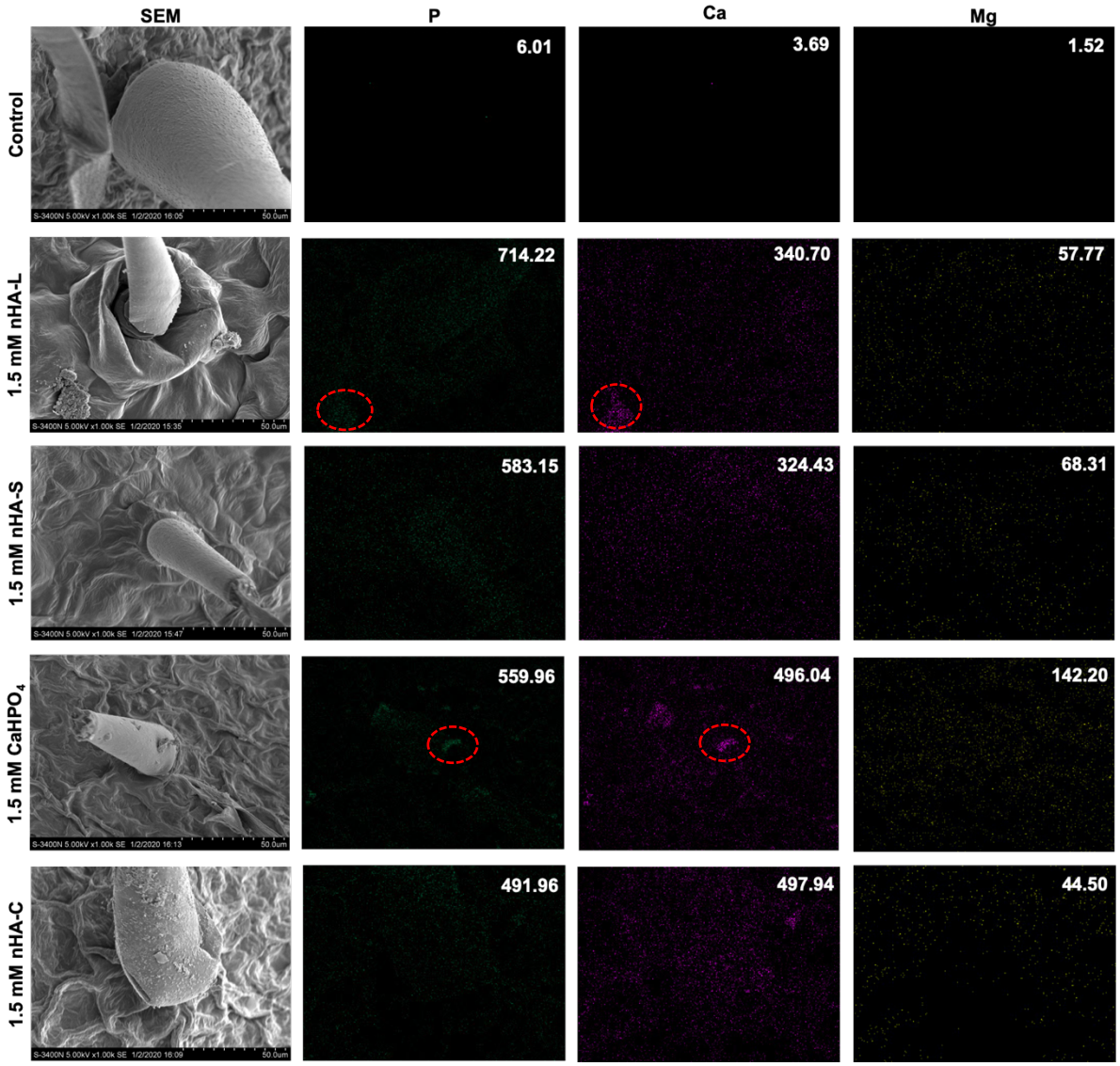

Figure S4. Particle distribution and energy dispersive spectra of P, Ca, Mg near trichomes of tomato leaves upon exposure to different sizes of nHA, or $CaHPO_4$ and commercial nHA.

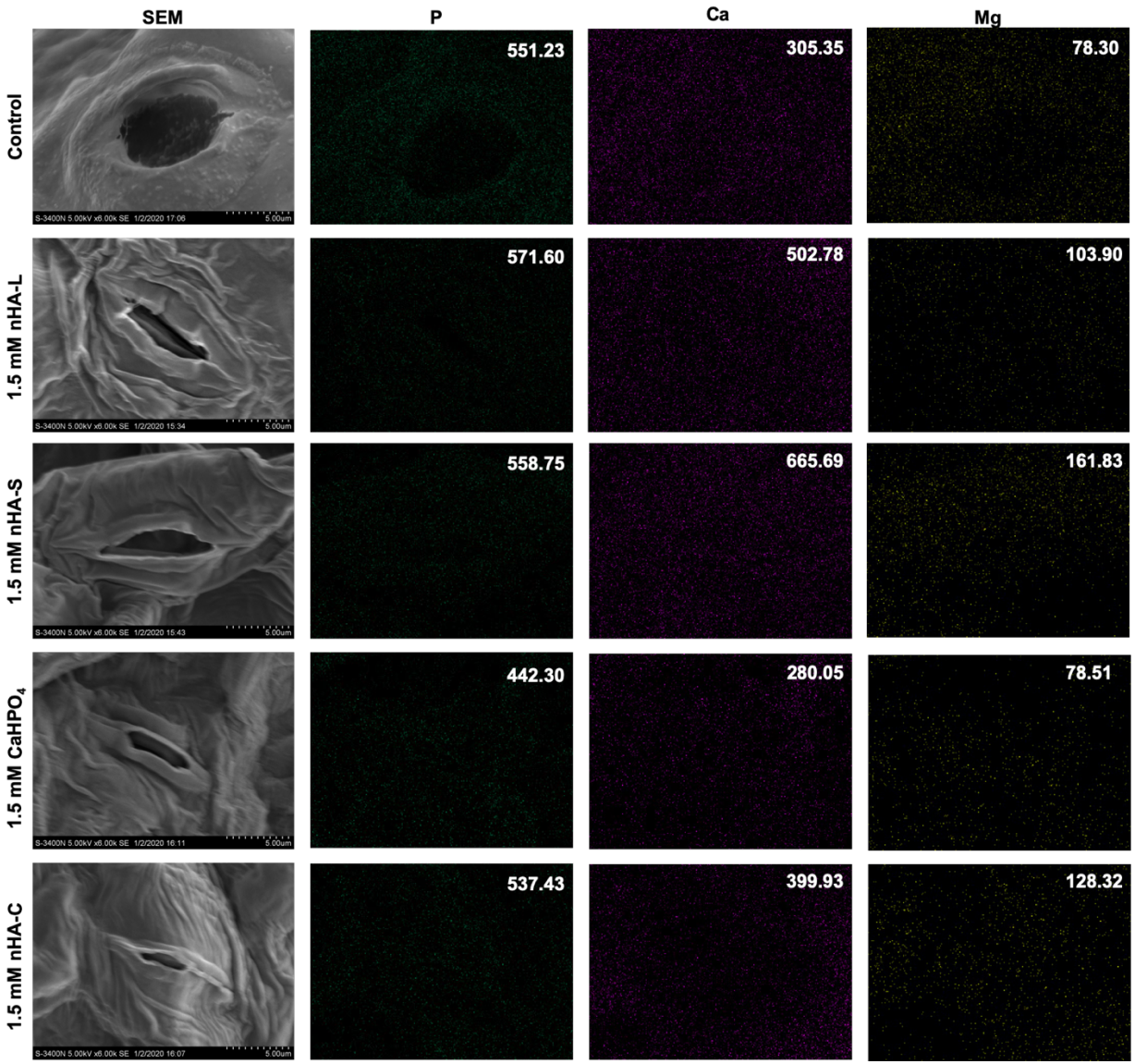

Figure S5. Particle distribution and energy dispersive spectra of P, Ca, Mg near stomata of tomato leaves upon exposure to different sizes of nHA, or $CaHPO_4$ and commercial nHA.

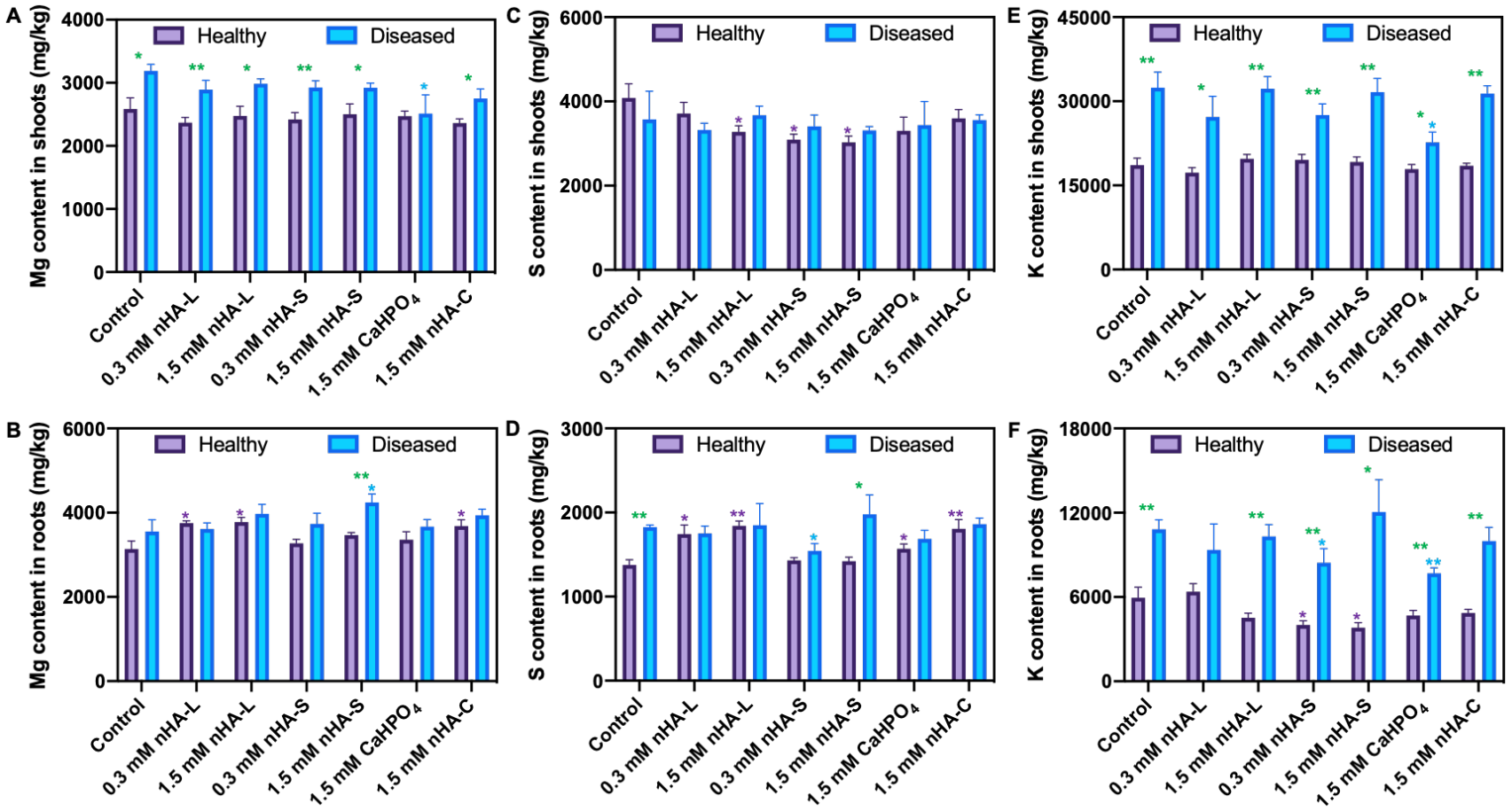

Figure S6. Mg (**A and B**), S (**C and D**) and K (**E and F**) content in tomato shoots and roots in healthy and diseased groups upon exposure to different sizes of nHA. In each panel, a single asterisk "*" and double asterisks "**" represents significant difference at $p < 0.05$ and $p < 0.01$, respectively; in addition, an asterisk in purple "*" indicates the significant difference between control and each nHA treatment within healthy group; asterisk in blue "*" indicates the significant difference between control and each nHA treatment within diseased group; asterisk in green "*" indicates the significant difference between healthy and diseased group within the same nHA treatment.

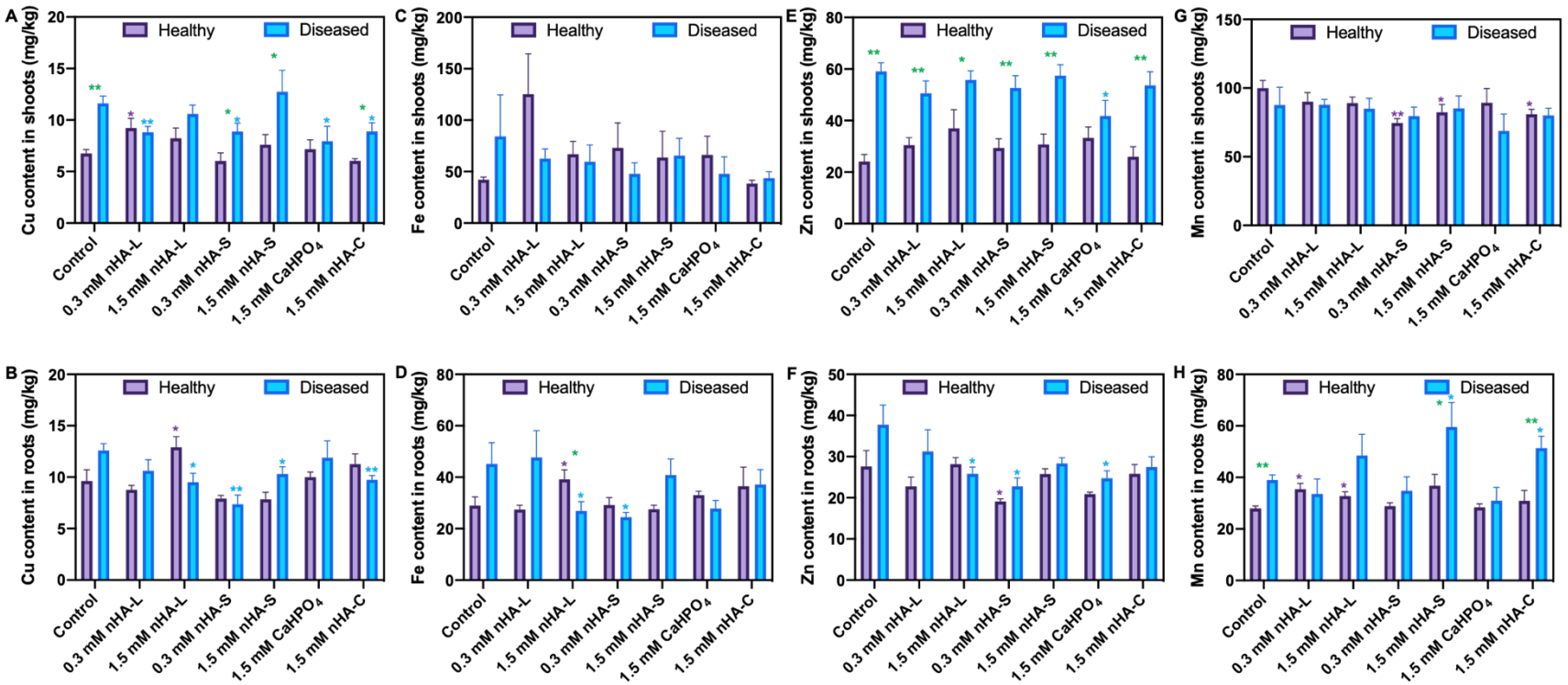

Figure S7. Micronutrient content in tomato shoots and roots in healthy and diseased groups upon exposure to different sizes of nHA. Figure **A and B**, **C and D**, **E and F**, **G and H** represents the contents of Cu, Fe, Zn, and Mn in tomato shoots and roots across all the treatments. In each panel, a single asterisk "*" and double asterisks "**" represents significant difference at $p < 0.05$ and $p < 0.01$, respectively; in addition, an asterisk in purple "*" indicates the significant difference between control and each nHA treatment within healthy group; asterisk in blue "*" indicates the significant difference between control and each nHA treatment within diseased group; asterisk in green "*" indicates the significant difference between healthy and diseased group within the same nHA treatment.

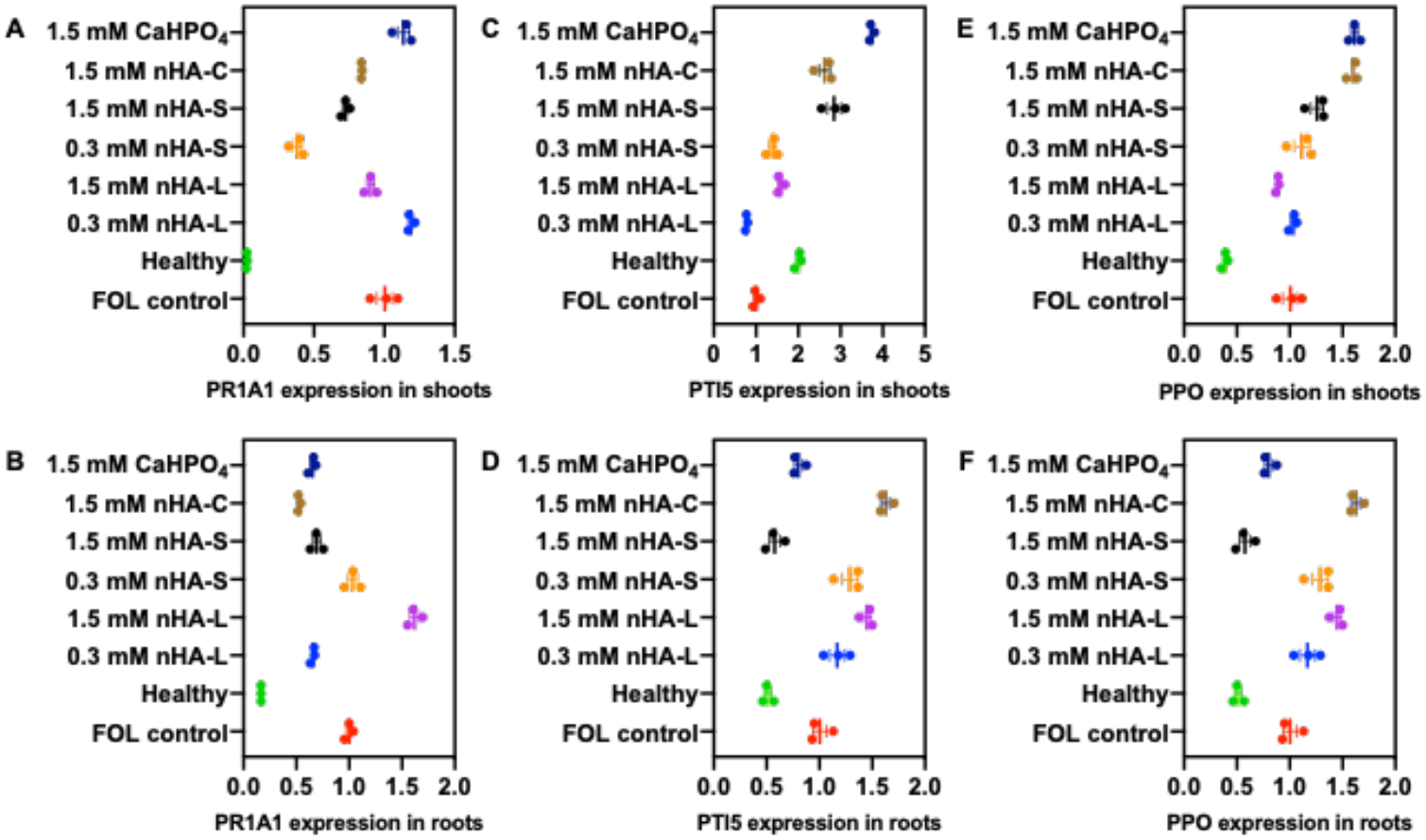

Figure S8. Relative expression of *PR1A1*(**A and B**), *PTI5* (**C and D**) and *PPO* (**E and F**) gene in *FOL* infected tomato shoots and roots upon exposure to different sizes of nHA. The diseased control is used to compare with each treatment and the healthy control as well.

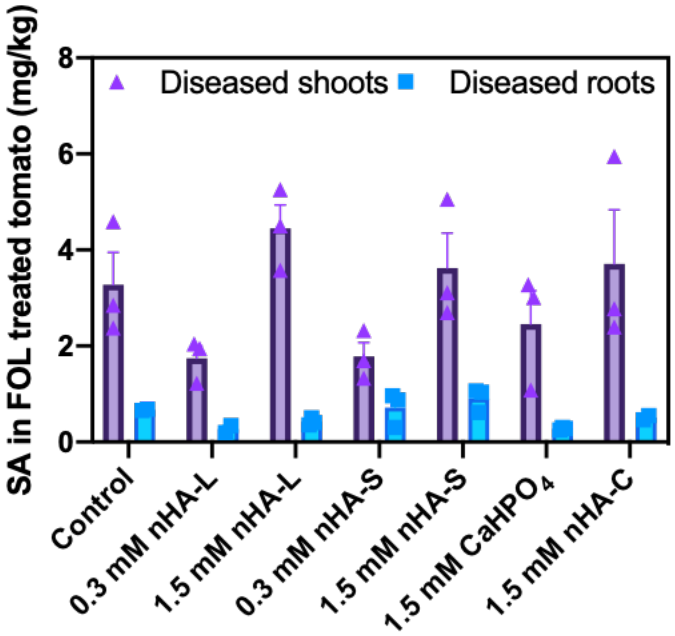

Figure S9. SA content in tomato shoots and roots in healthy and diseased groups upon exposure to different sizes of nHA. In each panel, a single asterisk "*" and double asterisks "**" represents significant difference at $p < 0.05$ and $p < 0.01$, respectively; in addition, an asterisk in purple "*" indicates a significant difference between control and each nHA treatment within healthy group; asterisk in blue "*" indicates the significant difference between control and each nHA treatment within diseased group; asterisk in green "*" indicates the significant difference between healthy and diseased group within the same nHA treatment.

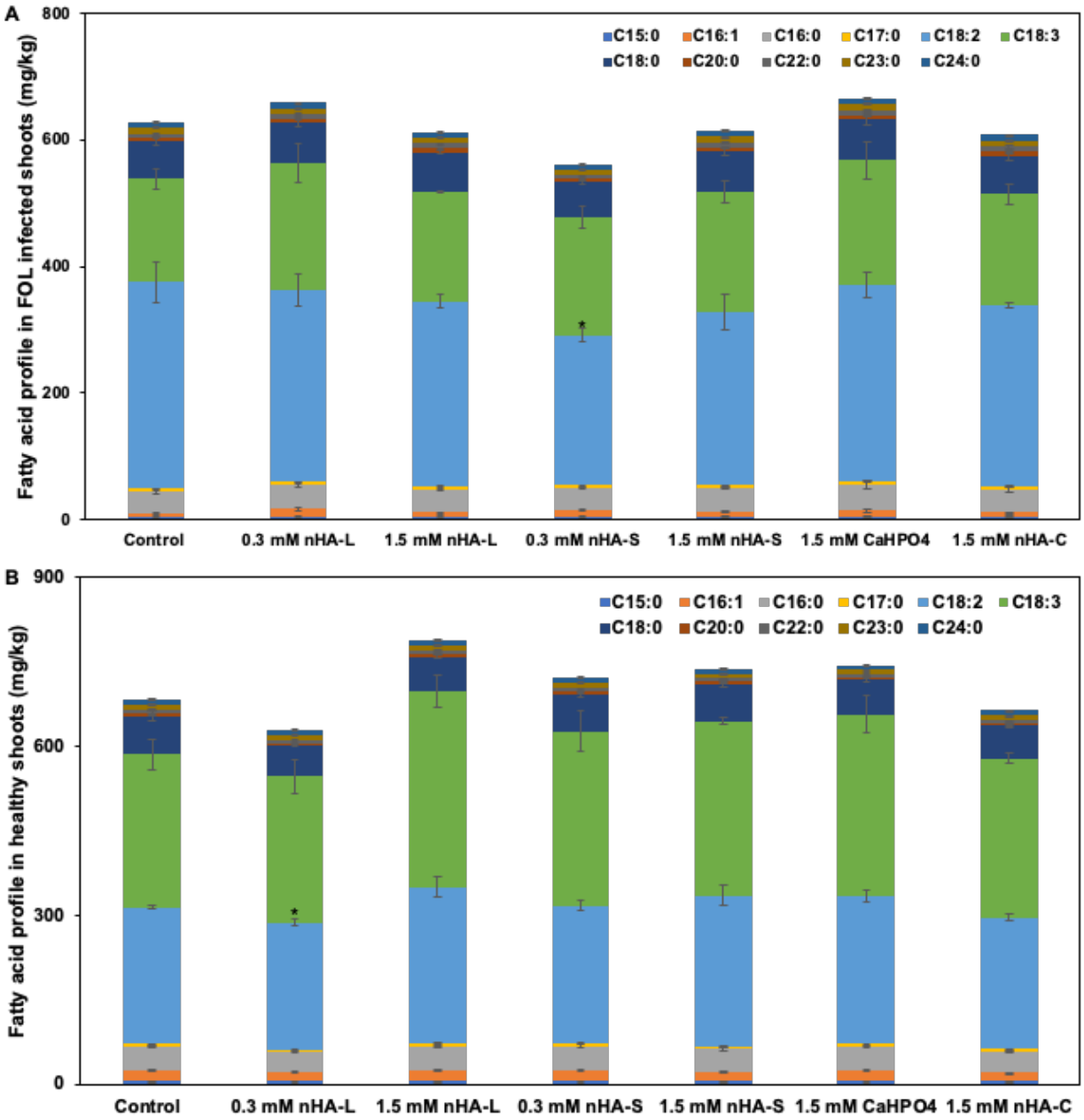

Figure S10. Fatty acid profile in tomato shoots in diseased (**A**) and healthy group (**B**) upon exposure to different sizes of nHA.

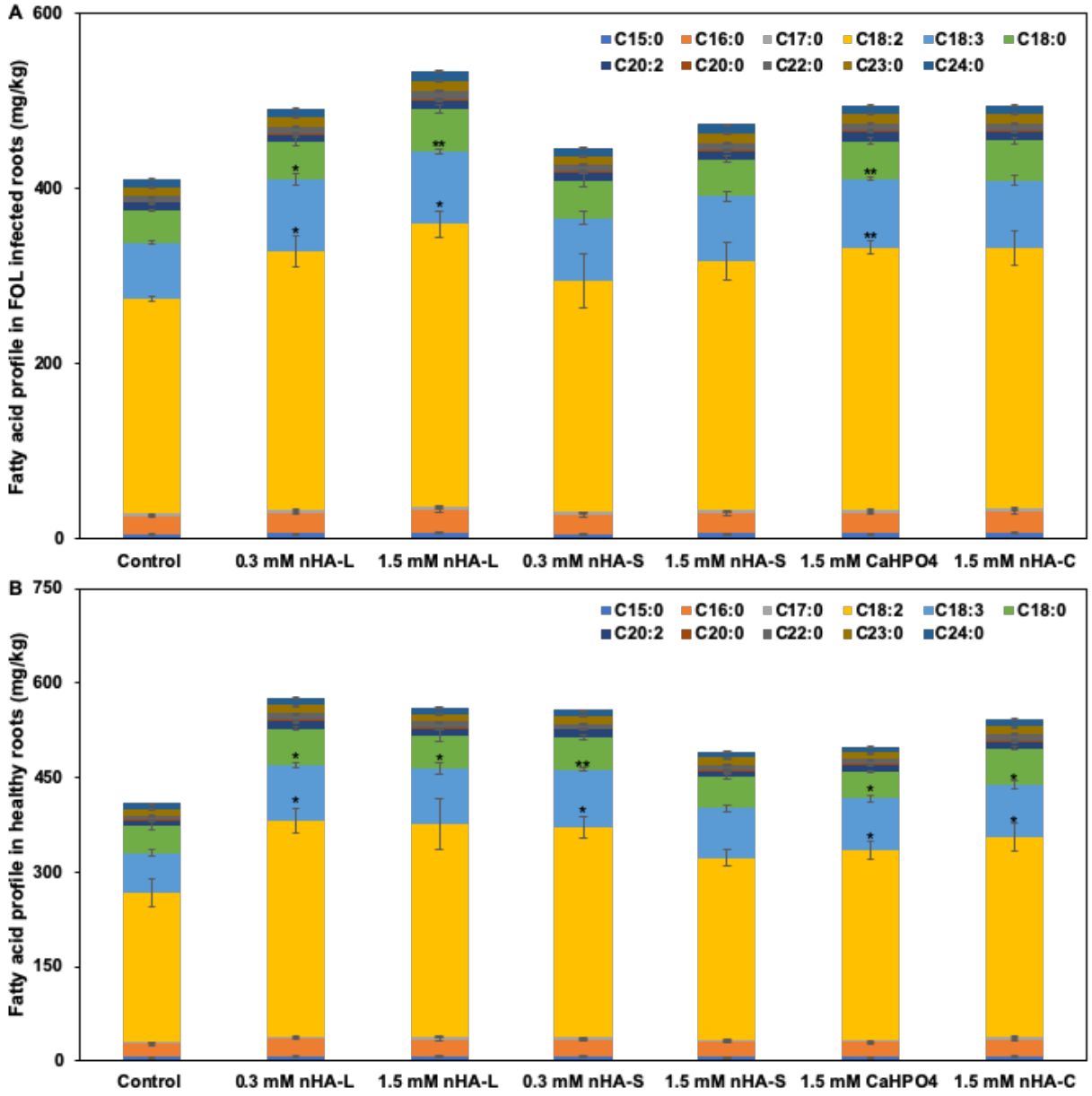

Figure S11. Fatty acid profile in tomato roots in diseased (**A**) and healthy group (**B**) upon exposure to different sizes of nHA.

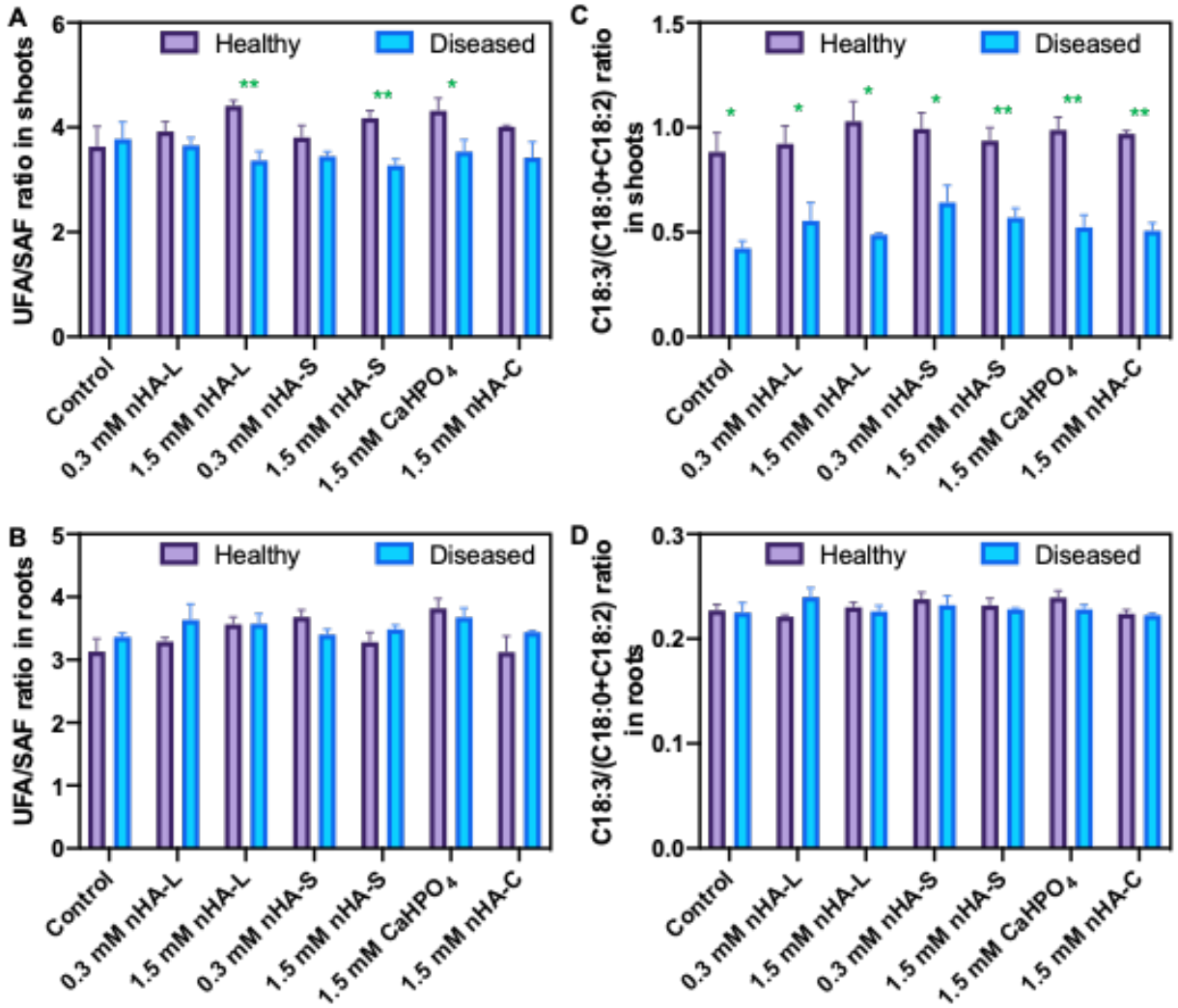

Figure S12. Ratio of UFA/SFA (**A and B**) andC18:3/(C18:0+C18:2) (**C and D**) in tomato shoots and roots in healthy and diseased groups upon exposure to different sizes of nHA. In each panel, a single asterisk "*" and double asterisks "**" represent significant difference at $p < 0.05$ and $p < 0.01$, respectively; in addition, an asterisk in purple "*" indicates the significant difference between control and each nHA treatment within the healthy group; asterisk in blue "*" indicates the significant difference between control and each nHA treatment within diseased group; asterisk in green "*" indicates the significant difference between healthy and diseased group within the same nHA treatment.

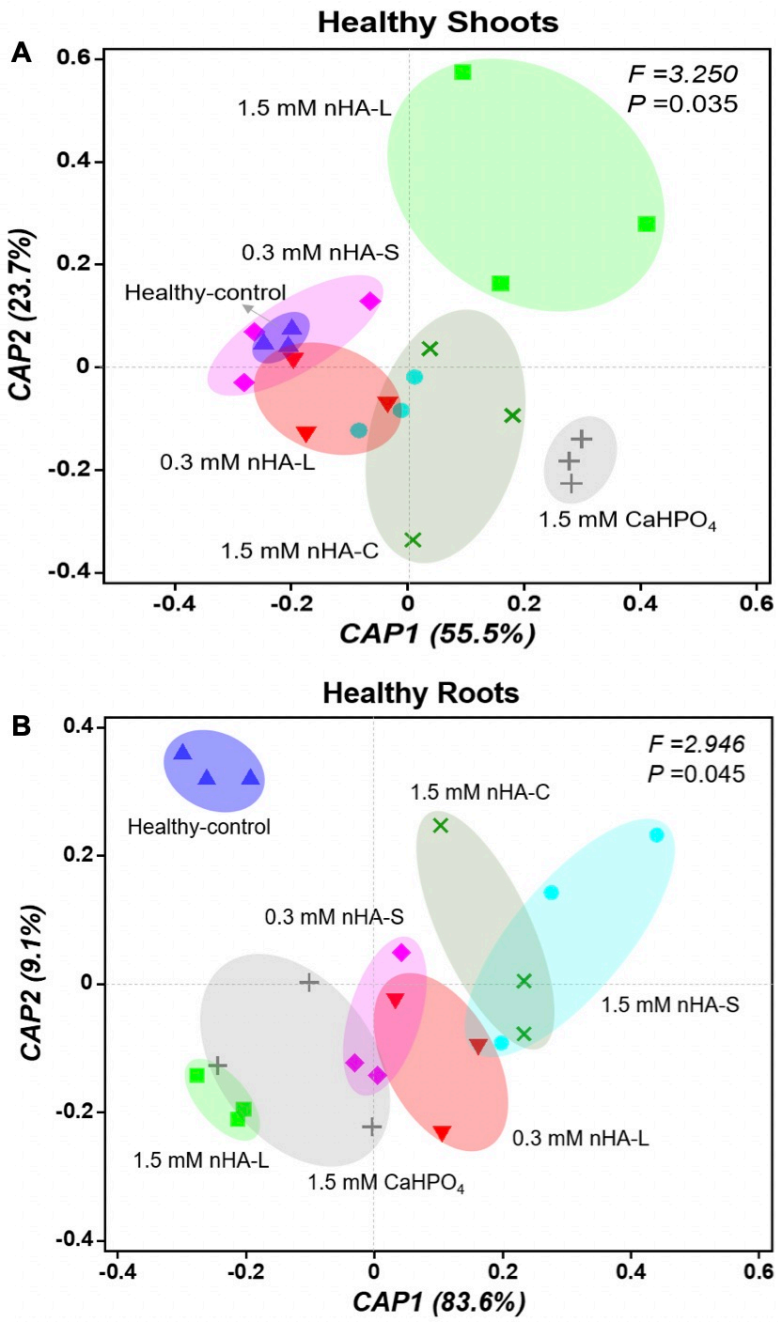

Figure S13. Ordination plots of fatty acid profile in shoots (**A**) and roots (**B**) in healthy groups upon exposure to different sizes of nHA. The dots in 2D ordination space indicate metabolite components at one sub-treatment in relationship to other sub-treatments. Dots located closer to each other share a larger percentage of metabolite components. The oval shadow contains all samples in the same treatments.

References:

1. Wang, T.T.; Ying, G.G.; Shi, W.J.; Zhao, J.L.; Liu, Y.S.; Chen, J.; Ma, D.D.; Xiong, Q. Uptake and Translocation of Perfluorooctanoic Acid (PFOA) and Perfluorooctanesulfonic Acid (PFOS) by Wetland Plants: Tissue- and Cell-Level Distribution Visualization with Desorption Electrospray Ionization Mass Spectrometry (DESI-MS) and Transmission Electron Microscopy Equipped with Energy-Dispersive Spectroscopy (TEM-EDS). *Environ Sci Technol* **2020**, *54*, 6009-6020, doi:10.1021/acs.est.9b05160.
2. Wang, Z.; Xu, L.; Zhao, J.; Wang, X.; White, J.C.; Xing, B. CuO nanoparticle interaction with Arabidopsis thaliana: toxicity, parent-progeny transfer, and gene expression. *Environmental science & technology* **2016**, *50*, 6008-6016.
3. Jing, G.; Huang, H.; Yang, B.; Li, J.; Zheng, X.; Jiang, Y. Effect of pyrogallol on the physiology and biochemistry of litchi fruit during storage. *Chemistry Central Journal* **2013**, *7*, 1-11.
4. Su, M.; Chen, K.; Ye, Z.; Zhang, B.; Guo, J.; Xu, C.; Sun, C.; Zhang, J.; Li, X.; Wu, A. Physical changes and physiological characteristics of red and green peel during nectarine (cv. Hu018) maturation. *Journal of the Science of Food Agriculture* **2012**, *92*, 1448-1454.
5. Zhao, L.; Hu, Q.; Huang, Y.; Fulton, A.N.; Hannah-Bick, C.; Adeleye, A.S.; Keller, A.A. Activation of antioxidant and detoxification gene expression in cucumber plants exposed to a Cu (OH) 2 nanopesticide. *Environmental Science: Nano* **2017**, *4*, 1750-1760.
6. Shang, H.; Ma, C.; Li, C.; White, J.C.; Polubesova, T.; Chefetz, B.; Xing, B. Copper sulfide nanoparticles suppress Gibberella fujikuroi infection in rice (Oryza sativa L.) by multiple mechanisms: contact-mortality, nutritional modulation and phytohormone regulation. *Environmental Science: Nano* **2020**, *7*, 2632-2643.
7. Le Guedard, M.; Schraauwers, B.; Larrieu, I.; Bessoule, J.J.J.E.t.; chemistry. Development of a biomarker for metal bioavailability: the lettuce fatty acid composition. **2008**, *27*, 1147-1151.
8. Guedard, M.L.; Schraauwers, B.; Larrieu, I.; Bessoule, J.J. Development of a biomarker for metal bioavailability: the lettuce fatty acid composition. *Environmental Toxicology and Chemistry: An International Journal* **2008**, *27*, 1147-1151.
9. Ma, C.; Borgatta, J.; De La Torre-Roche, R.; Zuverza-Mena, N.; White, J.C.; Hamers, R.J.; Elmer, W.H. Time-Dependent Transcriptional Response of Tomato (Solanum lycopersicum L.) to Cu Nanoparticle Exposure upon Infection with Fusarium oxysporum f. sp. lycopersici. *ACS Sustainable Chemistry & Engineering* **2019**, *7*, 10064-10074, doi:10.1021/acssuschemeng.9b01433.
10. Graham, R.D.; Webb, M.J. Micronutrients and disease resistance and tolerance in plants. *Micronutrients in agriculture* **1991**, *4*, 329-370.
11. Bonaventure, G.; Salas, J.J.; Pollard, M.R.; Ohlrogge, J.B. Disruption of the FATB gene in Arabidopsis demonstrates an essential role of saturated fatty acids in plant growth. *The Plant Cell* **2003**, *15*, 1020-1033.
12. Vassilev, A.; Lidon, F.; Scotti, P.; Da Graca, M.; Yordanov, I. Cadmium-induced changes in chloroplast lipids and photosystem activities in barley plants. *Biologia Plantarum* **2004**, *48*, 153-156.